




Synaptic potentiation dependence on spike variability

P. R. Protachevicz^{1,2,3,5,a} , M. S. Santos⁴, D. L. M. Souza⁵, L. E. Bentivoglio⁵, E. C. Gabrick^{2,5,6}, F. S. Borges^{5,7,8}, P. J. Abatti¹, A. M. Batista⁵, I. L. Caldas², and J. Kurths^{3,6}

¹ Graduate Program in Electrical Engineering and Industrial Informatics, Federal University of Technology, Curitiba, PR 80230-901, Brazil

² Institute of Physics, University of São Paulo, São Paulo, SP 05508-090, Brazil

³ Potsdam Institute for Climate Impact Research, Telegrafenberg A31, 14473 Potsdam, Germany

⁴ Municipal Secretary of Education of Ponta Grossa, Ponta Grossa, PR 84051-000, Brazil

⁵ Graduate Program in Science, State University of Ponta Grossa, Ponta Grossa, PR 84030-900, Brazil

⁶ Department of Physics, Humboldt University at Berlin, Berlin 12489, Germany

⁷ Department of Physiology and Pharmacology, State University of New York Downstate Health Sciences University, Brooklyn, NY 11203, USA

⁸ Center for Mathematics, Computation, and Cognition, Federal University of ABC, São Bernardo do Campo, SP 09606-045, Brazil

Received 18 August 2025 / Accepted 16 January 2026

© The Author(s) 2026

Abstract Understanding how the brain modifies synaptic connections and how firing patterns influence this process remains a major challenge in neuroscience. Aiming to clarify this relationship, we consider all-to-all neuronal networks with spike timing-dependent plasticity (STDP) where neurons are connected through excitatory chemical synapses with weak initial synaptic weights. We analyze how spike variability within a phase-synchronous pattern affects synaptic potentiation between neurons. Considering different methodologies, we find that, depending on the variability of spike synchronization and firing frequency, the potentiation of neuronal connections generates predominant unidirectional or bidirectional topologies. In addition, we identify four types of triad structures that are induced in the network. Particularly, for a certain level of variability in phase synchronization, a non-trivial optimization of the mean potentiation per spike is observed. In these cases, the potentiation occurs at a higher rate due to the preferential formation of unidirectional connections. Overall, our results deepen the knowledge of how phase firing patterns drive the synaptic changes in neuronal networks in the presence of STDP.

1 Introduction

Brain plasticity is directly involved in the learning, memory processes, and recovery from injuries [1, 2]. In simple terms, neuronal plasticity is described as the capability of synapses to change their intensity depending on the neuron activities [3]. In 1949, Donald Hebb proposed that the repeated co-activation of neurons that fire together leads to the strengthening of their synaptic connections [4]. Phenomenological models of plasticity are built on the rate or time of spikes [5]. In rate models, the firing frequency of the pre- and postsynaptic neurons determines the intensity of synaptic modification. On the other hand, in spike timing models, the synaptic modifications depend on the time at which spikes occur for the coupled neurons [1]. To study neuronal synchronization, plastic models that take into account time dependency are commonly used. A particular plasticity rule to guide these synaptic changes is spike timing-dependent plasticity (STDP) [6]. In this framework, synaptic changes depend on the spiking time of pre- and postsynaptic neurons. The STDP rule is based on experimental results mainly observed in the neocortex [7, 8] and hippocampus [9].

Phase synchronization is a dynamical phenomenon also related to brain learning [10], memory processes [11], and selective attention [12]. Particularly, transient phase synchronization has been reported in many studies about cognitive functions [13] such as those related to memory [14, 15], attention [12], and conscious perception [16]. By facilitating neuronal communication, synchronization supports efficient cognitive processing [17]. On the other

^a e-mail: protachevicz@gmail.com (corresponding author)

hand, abnormal synchronization or disrupted synchronization patterns [18] are recurrently associated with deficits in memory, attention, and cognitive processing [19]. Understanding how synchronous firing patterns drive neuronal connectivity is crucial in neuroengineering [20].

Many studies have been conducted to deepen our understanding of the effects of plasticity in neuronal networks. In 2004, Izhikevich et al. found that STDP and time delay generated the formation of spontaneous neuronal groups in a cortex network [21]. Wang et al. showed that a spiking neuronal network with resistive synapses learns how to identify different spatiotemporal patterns [22]. The resistance of the circuit components changes depending on the external stimuli, which is very similar to the plasticity mechanism in the brain. Yang et al. showed that synaptic plasticity induces longer chimera patterns [23]. In addition, chimera patterns are associated with complex configurations in the matrix of synaptic connections. Lameu et al. studied the effects of short-term and STDP in a conductance-based model [24]. They uncovered that neurons with similar spike frequency tend to establish connections more readily when considering both plasticities. The presence of delay in the synaptic current influences how plasticity regulates the synaptic inputs [25]. However, research that clarifies the role of particular firing patterns, such as phase synchronization, on structural modifications in recurrent networks with STDP remains insufficiently understood. Evidence suggests an interplay between synchronous patterns and synaptic modification [23, 26], but specific investigations addressing such characterization remain limited.

Different mathematical models such as the cellular automaton [27, 28], Rulkov [29, 30], Morris–Lecar [31], Galves–Löcherbach [32], Izhikevich [33], Hodgkin–Huxley [34], Hindmarsh–Rose [35], FitzHugh–Nagumo [36], and the integrate-and-fire [37] models have been proposed to describe the neuronal activity. One of the simplest mathematical models that combines biological plausibility with numerical efficiency is the adaptive exponential integrate-and-fire (AEIF) model [38]. This model exhibits spike adaptation and an exponential mechanism of spike initiation that enables the description of neuronal firing variability. This model was employed to study the emergence of epileptic seizures characterized by bistable states of synchronous and asynchronous activity [39]. Networks of AEIF neurons exhibit transitions between spike and burst patterns due to synaptic coupling as well as intrinsic spike and burst activities without coupling [40]. Zhang et al. reproduced a physiological network of the prefrontal cortex where the local activity is described by AEIF [41]. We consider in this study the adaptive exponential integrate-and-fire model due to the mathematical simplicity and direct parameter correlation with the biological neuronal mechanisms. The results obtained with this model can be reproduced by other neuronal models that present similar spike patterns.

Plasticity alters the strength of synaptic connections in the brain, and, as a consequence, the firing patterns exhibited by the neuronal network are also modified. In this work, we investigate this relationship in the opposite direction. We study how network firing patterns affect changes in synaptic weights. Particularly, we analyze how spike variability on phase synchronized patterns influences the synaptic modifications. The variability of phase synchronization quantifies how the synchronous pattern differs from complete phase synchronization. The level of variability affects the synaptic potentiation capacity. To investigate that, first we construct an all-to-all network composed of AEIF neurons connected by excitatory chemical synapses. Second, we select proper initial conditions to generate phase-synchronous patterns. Then, we include a Gaussian random dispersion in the initial conditions to explore the effect of the variability in the phase-synchronous patterns on the potentiation of neuronal connections.

As the main finding, we identify a region in the parameter space where the variability in phase-synchronous patterns can maximize the mean potentiation per spike. The results highlight the fundamental interplay between the effective learning rate, which governs the potentiation mechanism of neuronal synapses, and the spike variability, represented by the dispersion of phase-synchronous patterns. Our findings suggest that there is a range of spike variability in which the synaptic potentiation per spike is optimized, thereby enhancing the capacity of the network for plastic reconfiguration. Furthermore, we characterize how unidirectional and bidirectional network configurations emerge depending on the level of spike variability.

This paper is organized as follows. Section 2 introduces the network of coupled AEIF neurons, the spike time-dependent plasticity (STDP) rule, the initial conditions considered, the computation of the global order parameter, and the measurement of the mean synaptic weight and synaptic potentiation per spike. Section 3 presents the effects of neuronal firing patterns on the weight matrix. In Sect. 4, we discuss the main results and draw our conclusions.

2 Methods

2.1 Neuronal network dynamics

We consider an all-to-all connected neuronal network composed of $N = 100$ neurons that interact between themselves by means of excitatory chemical synapses. Auto-connections, called autapses, are not taken into account in this study [42]. At the single-cell level, the dynamics of each neuron is described by the adaptive exponential integrate-and-fire (AEIF) model [38]. The AEIF model consists of two variables, the membrane potential and the adaptive current. The exponential term in the equation of membrane potential describes the threshold that

the membrane needs to achieve to fire an action potential [38, 43]. The slow dynamics of potassium ion channels are described by the adaptation current [43]. In this model, an equation for synaptic conductance is included to describe the intensity of interaction between the neurons. The AEIF model is described by the following equations:

$$\begin{aligned}
 C_m \frac{dV_j}{dt} &= -g_L(V_j - E_L) + g_L \Delta_T \exp\left(\frac{V_j - V_T}{\Delta_T}\right) \\
 &\quad - w_j + I_0 + (V_{\text{rev}} - V_j) \sum_{k=1}^N g_k M_{jk}, \\
 \tau_w \frac{dw_j}{dt} &= a(V_j - E_L) - w_j, \\
 \tau_s \frac{dg_j}{dt} &= -g_j,
 \end{aligned} \tag{1}$$

where V_j , w_j , and g_j correspond, respectively, to the neuronal variables: membrane potential, adaptation current, and synaptic conductance from the neuron j , and t is the time variable in milliseconds (ms). The constant parameters are C_m (membrane capacitance), g_L (leak conductance), E_L (resting potential), Δ_T (slope factor), V_T (spike threshold potential), I_0 (constant current applied), V_{rev} (synaptic reversal potential), τ_w (adaptation time constant), a (sub-threshold adaptation level), and τ_s (synaptic time constant). The elements of the weight matrix M_{jk} assume values higher than 0 when presynaptic (k) and postsynaptic (j) neurons are connected, and 0 when they are not.

In this model, when V_j exceeds the threshold potential ($V_j > V_{\text{th}}$) [43], the neuron fires, and the variables V_j , w_j and g_j are updated by the following reset rules:

$$\begin{aligned}
 V_j &\rightarrow V_r, \\
 w_j &\rightarrow w_j + b, \\
 g_j &\rightarrow g_j + 1,
 \end{aligned}$$

where V_r is the reset potential and b is the over-threshold adaptation parameter. In this work, we consider that the synaptic conductance assumes a maximal unitary value due to the neuron spike j . In our simulations, we set $C_m = 200$ pF, $g_L = 12$ nS, $E_L = -70$ mV, $\Delta_T = 2$ mV, $V_T = -50$ mV, $\tau_w = 300$ ms, $a = 2$ nS, $\tau_s = 2.728$ ms, $V_{\text{rev}} = 0$ mV, $V_r = -58$ mV, and $b = 70$ pA. For the results showing the neuronal dynamics, individual synaptic intensities and weight distributions, we consider $I_0 = 500$ pA. For diagnostics in the parameter space, we consider I_0 in the range [300,1000] pA. For high frequencies, the synaptic intensity can build-up in the synaptic transmission as it has no time to relax to low values. However, in our simulations, the constant decay time of g_j is small enough (equal to 2.728 ms), to generate a fast decay of the synaptic transmission, and such build-up does not occur. The fast decay time prevents conductance buildup and emphasizes the temporal precision of synaptic transmission. The chosen value $\tau_s = 2.728$ ms is still consistent with previous computational models studying AMPA receptors that allow us to model the neuronal dynamics while avoiding artifacts from the cumulative conductance [44, 45].

2.2 Spike time-dependent plasticity (STDP)

Spike timing-dependent plasticity (STDP) is a process that changes the synaptic strengths depending on the neuron spike time. For each synaptic connection, the spike times of pre- and postsynaptic neurons are identified as t_k and t_j , respectively. When a neuron spike occurs, an update in the synaptic intensity is considered. The changes in the synaptic weights ΔM_{jk} depend on the time difference $\Delta t_{jk} = t_j - t_k$ and is given by [9]

$$\Delta M_{jk} = \begin{cases} A_1 e^{(-\Delta t_{jk}/\tau_1)} & , \text{ if } \Delta t_{jk} \geq 0, \\ -A_2 e^{(\Delta t_{jk}/\tau_2)} & , \text{ if } \Delta t_{jk} < 0, \end{cases} \tag{2}$$

where $A_1 = 1$ nS, $A_2 = 0.5$ nS, $\tau_1 = 1.8$ ms, and $\tau_2 = 6$ ms [46]. When the neuron j spikes, all neurons k connected with the neurons j , from $j \rightarrow k$ and $k \rightarrow j$ are updated by Eq. (2). We modify the synaptic weight of the connection from neuron k to j when $t_k > t_j$ or when $t_k < t_j$, based on the synaptic plasticity model. Notice that the indices k and j represent a neuron that has a connection from neuron k to neuron j . In addition, the synaptic rule is applied for the last spike of neuron j and k in the simulation. The synaptic weights are updated according to Eq. (2), where $M_{jk} \rightarrow M_{jk} + \eta \Delta M_{jk}$, in which $\eta = 10^{-3}$ identifies the learning rate. In this work, we consider a small initial value for the synaptic weight equal to $M_{jk}^{\text{ini}} = 0.001$ nS for $j \neq k$, and $M_{jk}^{\text{ini}} = 0$ for $j = k$. The synaptic connections are lower limited on $M^{\text{min}} = 0$ and upper bounded on $M^{\text{max}} = 1$ nS, i.e., $M_{ij} = [M^{\text{min}}, M^{\text{max}}]$.

2.3 Initial conditions of the neuronal variables

The initial conditions of the neuron variables are chosen aiming for the neuronal dynamics to exhibit phase synchronization, desynchronization, or intermediate levels of spike synchronization. For phase synchronization, we choose equal values for the neuronal variables, $V_j(0) = E_L$ and $w_j(0) = b$. To induce dispersion in the initial condition that generates variability in the phase-synchronous patterns, we consider the equation

$$w_j(0) = b + G(\mu = 0, \sigma), \quad (3)$$

where $G(\mu = 0, \sigma)$ is a Gaussian random number generator with mean $\mu = 0$ and standard deviation σ . The effect of dispersion in the membrane potential on the variability in phase-synchronous patterns is small when compared to the dispersion considered in the adaptation current. For this reason, we take into account a dispersion only in the adaptation current variable. We consider the parameter associated with the dispersion in the initial condition in the following range $\sigma = [0, 20]$ pA. For $\sigma = 0$, no random variability is included in the initial conditions. As the value of σ increases, the random Gaussian variability is added to the initial condition of the firing patterns. For large σ , e. g., $\sigma = 20$ pA, the network exhibits desynchronized activities. As the neuronal network is weakly coupled, the firing pattern associated with the spike dynamics is initially determined by the initial conditions, which makes it possible to study the influence of the pattern on the potentiation of synapses related to network structure.

2.4 Global order parameter

To study the phase synchronization level [47] of the neuronal network, we analyze the mean global order parameter \bar{R} [48], defined as

$$\bar{R} = \frac{1}{t_{\text{fin}} - t_{\text{ini}}} \int_{t=t_{\text{ini}}}^{t_{\text{fin}}} \left| \frac{1}{N} \sum_{j=1}^N e^{i\phi_j(t)} \right| dt, \quad (4)$$

where $t_{\text{ini}} = 0$ s and $t_{\text{fin}} = 5$ s are, respectively, the initial and final time of simulation, and “i” is the imaginary number. The phase of each neuron $\phi_j(t)$ is defined in terms of two consecutive spikes of each neuron j by

$$\phi_j(t) = 2\pi \frac{t - t_j^l}{t_j^{l+1} - t_j^l}, \quad (5)$$

where t_j^l is the l -th spike time of the j -th neuron. $\phi_j(t)$ is defined in the interval $[t_j^l, t_j^{l+1}]$. We use \bar{R} as a diagnostic of the levels of phase synchronization. \bar{R} close to 1 identifies a high level of phase synchronization, while \bar{R} close to 0 is associated with asynchronous spikes.

2.5 Mean synaptic weight

We quantify the mean synaptic weight of the neuronal network, $\bar{M}(t)$, by

$$\bar{M}(t) = \frac{1}{N(N-1)} \sum_{j, k, j \neq k}^N M_{jk}(t), \quad (6)$$

where M_{jk} are the synaptic weights for each connection from neuron j to k . For this measure, only non-null initial connections are included in such calculation, where by definition, the null ones are the auto-connections ($j = k$). Notice that Eq. (4) can be applied to $t = 0$ until $t = 5$ s. To calculate the mean synaptic weight in the final simulation time, we use $t = 5$ s in Eq. (6). This period is sufficient to observe the trend in synaptic weight modifications resulting from firing patterns.

2.6 Mean synaptic potentiation per spike

Due to the dependence of plasticity rule on the spike events, we could expect that high frequencies have more changes in the synaptic weights than low ones. To monitor the mean change of the synaptic weight during the

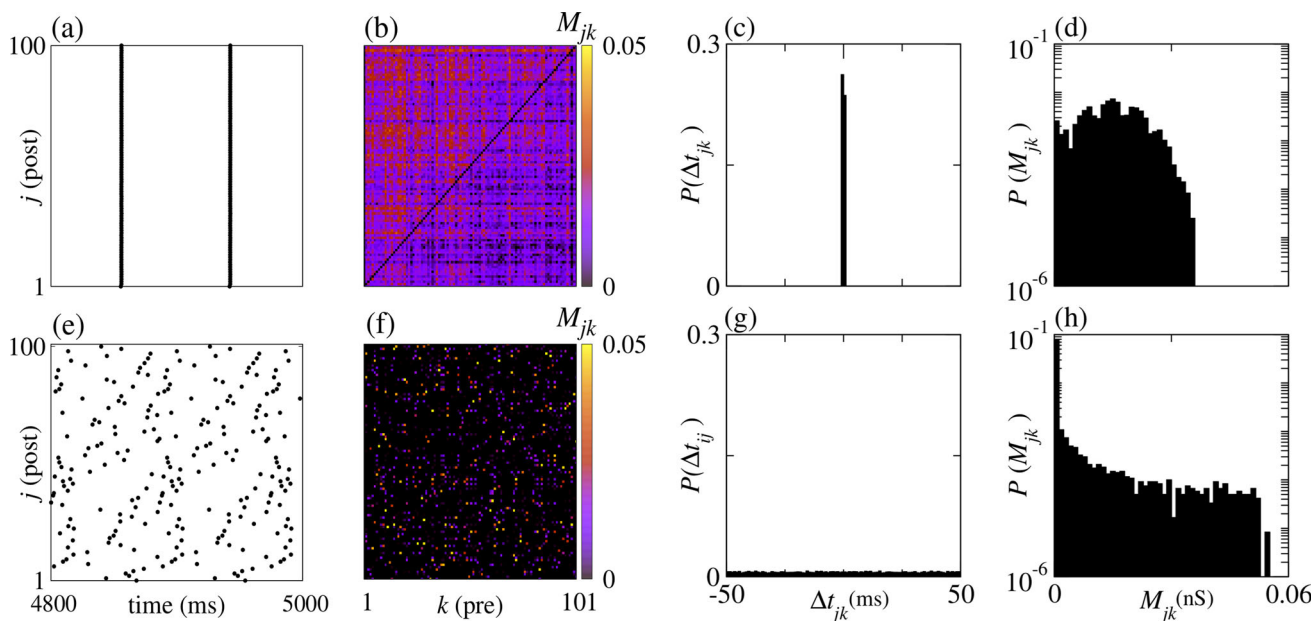


Fig. 1 **a** Raster plot, **b** the respective weight matrix of synaptic connections (in $t = 5$ s), **c** the spike interval between the pre and postsynaptic neurons, and **d** the synaptic weights associated with the synchronous patterns. The same diagnostics for the case of desynchronous patterns are shown in the panels (**e–h**). In (**a–d**), we consider $\sigma = 0.001$. In (**e–h**), we consider $\sigma = 10$

simulation independently of the mean firing frequency, we analyze the potentiation of the mean synaptic intensity per spike, defined as

$$\bar{P} = \frac{\Delta \bar{M}}{N_{\text{spikes}}} = \frac{\bar{M}^{\text{fin}} - \bar{M}^{\text{ini}}}{\bar{F} \cdot T}, \tag{7}$$

where \bar{M}^{ini} and \bar{M}^{fin} are the initial and final mean value of the weight matrix, respectively, and N_{spikes} is the number of spikes during the simulation. The potentiation per spike can be obtained directly from the diagnostics of the network, taking into account the mean synaptic change ($\Delta \bar{M}$), the mean spike frequency (\bar{F}), and the period (fixed on $T = 5$ s) of the simulation. In Eq. 7, the values of $\Delta \bar{M} > 0$ correspond to mean potentiation while $\Delta \bar{M} < 0$ corresponds to mean depression. In this work, the synaptic weights are typically potentiated. The mean synaptic potentiation per spike reflects the rate of synaptic increase per spike, depending on the firing patterns. This is important for understanding how the firing patterns act to strengthen synaptic connections. High rates of potentiation indicate that the neuronal network is self-organizing, while small mean changes may indicate that the network regimes approximate a stationary state.

3 Results

3.1 Phase-synchronous and asynchronous patterns

Figure 1 shows the raster plot (spike times) of (a) phase synchronized pattern ($\sigma = 0.001$ pA) and (b) the associated synaptic weight matrix, (c) the distribution of time differences between the neurons, and (d) the distribution of synaptic weights generated due to the phase-synchronous pattern. Figures 1(e-h) exhibit the same diagnostics presented for phase-synchronous patterns, however, for the desynchronous pattern ($\sigma = 10$). For synchronous patterns (Fig. 1a), the synaptic potentiation occurs in an almost bidirectional way (Fig. 1b) because Δt_{jk} is close to 0 (Fig. 1c), being associated with a predominant synaptic potentiation from the initial value, as observed in Fig. 1d. For desynchronous patterns, corresponding to the initial condition with high dispersion, as shown in Fig. 1e, a large number of synaptic connections are maintained in the initial values or they go to zero (Fig. 1f). Some connections are potentiated due to statistical coincidences of spikes. For the desynchronous patterns, the

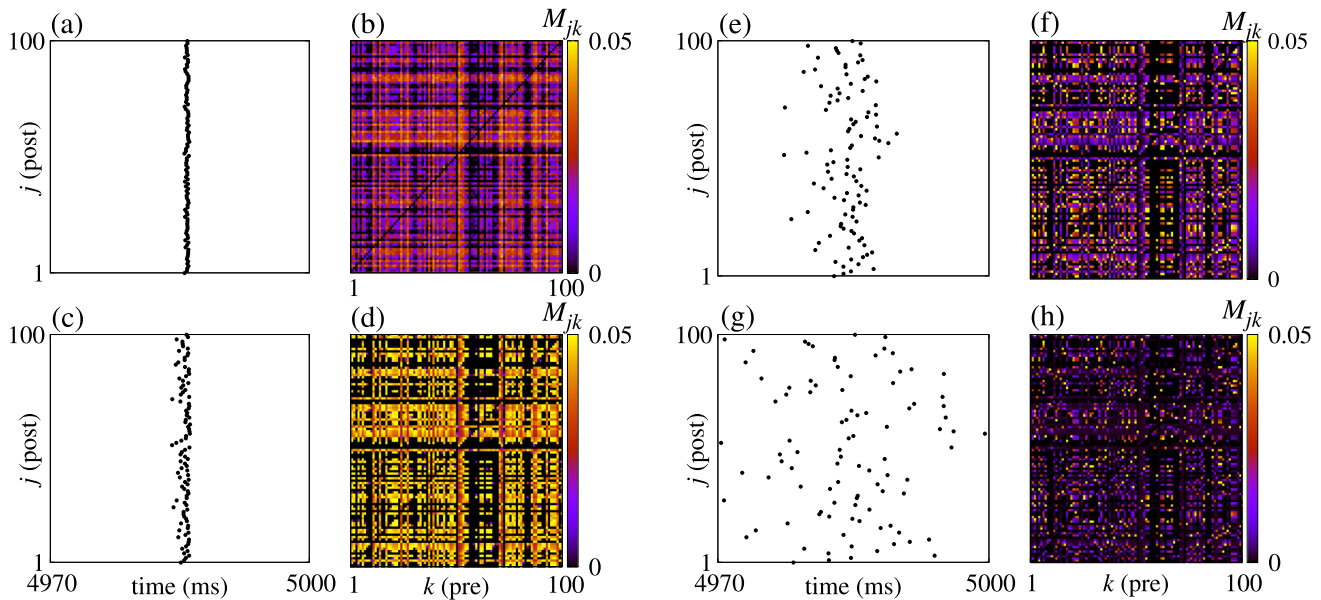


Fig. 2 Raster plots of the neuronal activities and synaptic matrices for $t = 5$ s for different dispersions in the initial conditions of neurons for the phase-synchronous pattern considering $I_0 = 500$ pA. Level of dispersion in the firing patterns equal to **a, b** $\sigma = 0.01$ pA, **c, d** $\sigma = 0.48$ pA, **e, f** $\sigma = 3.0$ pA, and **g, h** $\sigma = 8.0$ pA. σ stands for the standard deviation in the initial conditions in the w_i variables

spike intervals between the neurons are spread in different values (Fig. 1g), generating the concentration in the synaptic weight at the zero value (Fig. 1h).

3.2 Dispersion in synchronous phase patterns

To deepen the knowledge about the influence of such patterns in the synaptic changes, we focus on the transition from phase synchronous to desynchronous spikes for different frequencies and levels of variability in the phase-synchronous pattern. We investigate the effect of variability in the phase-synchronous patterns on the weight matrix modification in the presence of STDP. Considering a small dispersion in the initial condition ($\sigma = 0.01$), a small variability in the phase-synchronous pattern is observed (Fig. 2a). Such variability generates potentiation and depression of different connections. In such case, the connections that are potentiated and depressed are spread on the weight matrix (Fig. 2b). In this case, it is possible to identify neurons that are strongly potentiated in their incoming and/or outgoing synaptic connections, as well as neurons where such connections are depressed to zero. If we consider $\sigma = 0.48$ pA, the firing patterns shown in Fig. 2c appear. The weight matrix generated by such a pattern is similar to the previous one, however, more connections go to zero or to higher values (Fig. 2d). In such a case, many connections are potentiated approximately to a 0.05 value. As the dispersion in the initial condition increases, e.g., $\sigma = 3$ pA and $\sigma = 8$ pA, the variability in phase-synchronous patterns also increases (Fig. 2e and g), respectively. The number of connections that assume low or zero values increases (Fig. 2f and h). If a higher σ is considered, e.g., $\sigma = 20$ pA, desynchronous patterns (Fig. 1e) are obtained.

After observing that the different levels of variability in the firing patterns has a deep influence on the synaptic potentiation of the connections, we investigate how such variability is related to the potentiation over time. Figure 3a shows the mean synaptic weight over time due to different dispersions of phase-synchronous patterns (Fig. 2). As observed in Fig. 3a, a level of dispersion close to zero ($\sigma = 0.01$ pA - black line) has a higher potentiation per spike than a pattern with higher variability (e. g., $\sigma = 3$ pA and 8 pA, green and blue line, respectively). However, for a certain value of variability in the phase-synchronous pattern ($\sigma = 0.48$ pA), we observe the highest potentiation per spike when we analyze the mean synaptic weight. Such results mean that the mean value of the connections potentiates with different rates per spike during the initial transient time according to the level of synchronization. In addition, depending on the frequency, a certain level of variability in the phase-synchronous pattern can be associated with the highest potentiation per spike. Figure 3b–e displays the respective synaptic weight distributions for each pattern exhibited in Figs. 2 and 3. In the inset of Fig. 3b–e, we add the distribution of spike times between neurons that are directly related to the synaptic changes in Eq. 2.

The mean weight values of the synaptic connections over 5 h are shown in the inset of Fig. 3a. The increase in the synaptic connection intensities can change the dynamics of the network, which do not allow us to conclude about the effect of the levels of phase-synchronous patterns on the synaptic modifications. However, for the

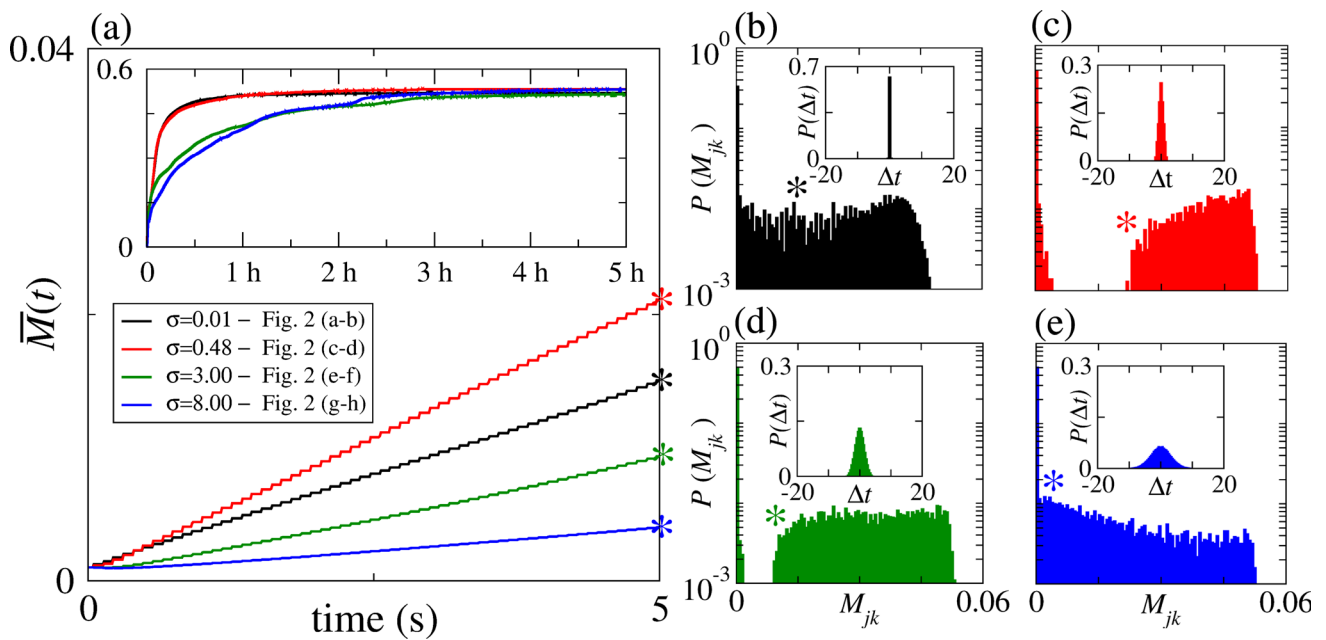


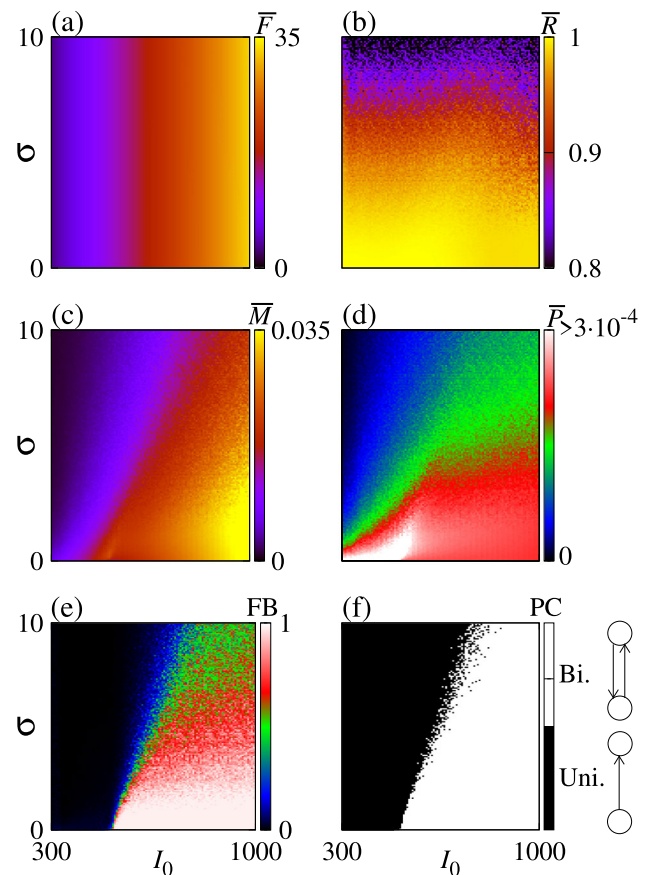
Fig. 3 **a** Mean synaptic weight over time considering different levels of dispersion in the initial condition. The inset shows the convergence of the mean weight value over a period of 5 h. Synaptic weight distribution related to the panel **a** for **b** $\sigma = 0.01$ pA, **c** $\sigma = 0.48$ pA, **d** $\sigma = 3.0$ pA and **e** $\sigma = 8.0$ pA after 5 s. The insets show the spike difference between the neurons due to the initial conditions. The colored asterisks in (a) stand for the time at which the synaptic distributions in (b), (c), (d), and (e) are considered. In (b), (c), (d) and (e), the asterisks represent the mean value of the weight distribution

transient and short time analysis, it is possible to draw a conclusion about the effect of firing patterns on the synaptic modification. We choose the first 5 s of simulation to study the synaptic potentiation to avoid significant modifications in the level of phase synchronization due to chemical connection interactions. After some time, for example $t > 25$ s, the synaptic interactions in the network modify the variability of phase synchronization, and drive synaptic changes with different mean potentiation per spike, a fact that can be seen in the inset of Fig. 3a. It is worth mentioning, that the intensities of connections are small to considerably affect the variability of phase synchronization for a short transient time, although the influence of the network on the dynamics is still present. In this way, there is a predominant influence of the dynamics on the synaptic modification, but a small influence of structure on the synchronized patterns.

Figure 4 shows the diagnostics of dynamics and measurements associated with the mean synaptic weight. Figure 4a exhibits the mean spike frequency. As can be seen there, the dispersion in the initial condition associated with σ , that increases the variability of phase-synchronous patterns, does not change the firing frequency, and the constant current applied determines the mean spike frequency. On the other hand, the synchronization level is not affected considerably by the constant current. The dispersion σ in the initial condition modifies the variability of the phase synchronization. This fact is seen in Fig. 4b by the values of the mean order parameter \bar{R} . However, as observed in Fig. 4c, the mean synaptic value achieved after 5 s, depends on the combination of the spike frequency (generated by the constant applied current) and the variability of spikes (generated by the dispersion of the initial conditions). We note that the lowest firing frequencies and highest dispersion are associated with the smallest mean synaptic potentiation. Otherwise, higher frequencies with small variability are associated with the highest potentiation level. However, since more updates can generate more potentiation on time due to a high spike frequency, we also consider the mean potentiation per spike. This measure offers a diagnostic of synaptic connections potentiation adjusted by the mean spike frequency. In turn, the spike frequency is directly related to the number of spikes in each second. In this way, it is possible to identify the dynamics that contribute more to the potentiation of individual spikes on average. Such a measurement is shown in Fig. 4d. We also find that a low frequency can potentiate (on average) more per spike for small dispersion in phase synchronization than for a higher spike frequency. In addition, we notice that not necessarily a smaller variability in phase synchronization potentiates more per spike. Further details are provided in Fig. 5.

We also investigate the fraction of bidirectional connections and the predominance of the connectivity due to different variabilities of phase synchronization. In the simulation, we identify a connection as unidirectional between two neurons when only one connection of the pair has a value equal to or greater than the initial value $M_{ij}^{\text{init}} = 0.001$ nS. Analogously, we identify a bidirectional connectivity between two neurons when both connections of the pair have a value equal to or greater than the initial value $M_{ij}^{\text{init}} = 0.001$ nS. Figure 4e and f shows the fraction

Fig. 4 Diagnostics of the dynamics and mean synaptic weight in the parameter space of $\sigma \times I_0$. (a) Mean firing frequency, (b) global order parameter, (c) mean synaptic weight, (d) mean synaptic potentiation per spike, (e) fraction of bidirectional connections in the network, and (f) predominance of connections in unidirectional or bidirectional configuration between pairs of neurons in the network. Next to the “Bi.” (bidirectional) and “Uni.” (unidirectional) labels, schematic diagrams with circles and arrows illustrate each structure



of bidirectional connections (FB) and the predominance connectivity (PC) of unidirectional and bidirectional connections, respectively. In these figures, we observe that the potentiation of predominant unidirectional and bidirectional connectivity is related to the firing frequency and the variability of phase synchronization. Lowest frequencies are associated with predominant unidirectional connectivity, while higher frequencies are associated with bidirectional ones. In addition, the increase in the variability of phase synchronization can reduce the fraction of potentiation in a bidirectional way (Fig. 4e).

To observe closely the possible optimization effect of the potentiation per spike due to the variability, we refine our analysis of the mean potentiation per spike (\bar{P}) and the synaptic weights distributions. Figure 5a shows \bar{P} for $I_0 = 300$ pA (black line), $I_0 = 500$ pA (red line) and $I_0 = 700$ pA (blue line). A certain variability in the phase-synchronous patterns generated by dispersion on the initial conditions can improve the potentiation of the synaptic connection per spike for $I_0 = 300$ pA, $I_0 = 500$ pA and $I_0 = 700$ pA. We plot the distribution of the synaptic weights for four parameters indicated in Fig. 5a by red circles. In the inset of Fig. 5b–e, the distribution of the spike intervals between the neurons is shown for each parameter $\sigma = 0.03$ pA, $\sigma = 0.22$ pA, $\sigma = 1.0$ pA and $\sigma = 1.5$ pA. The variability of spike due to the dispersion for $\sigma = 0.22$ pA generates a larger amount of the highest synaptic weights compared with the other cases, as indicated by the red arrow in Fig. 5c. For the other values of σ shown in Fig. 5b, d and e, respectively, the distribution of the synaptic weights does not assume a concentration in the highest values. We consider distinct parameters in Fig. 5 to show a different scenery from Fig. 3. Figure 3 exhibits the effect of dispersion in the phase synchronization on the potentiation rate over time in a broader context. Figure 5 focuses on a specific result observed in parameter space ($\sigma = [0, 2]$ pA), where a certain value of dispersion and frequency (associated with I_0), can optimize the potentiation.

4 Network metrics

For in-depth understanding of the structure generated in the matrix due to the dispersion and external current, we consider the principal component analysis (PCA) and the use of the cluster method (K-means). To apply it, we consider the Scikit-Learn library [53]. The objective is to identify relevant differences between the synaptic connections represented in the matrices. The analysis starts with the collection of the synaptic weights derived

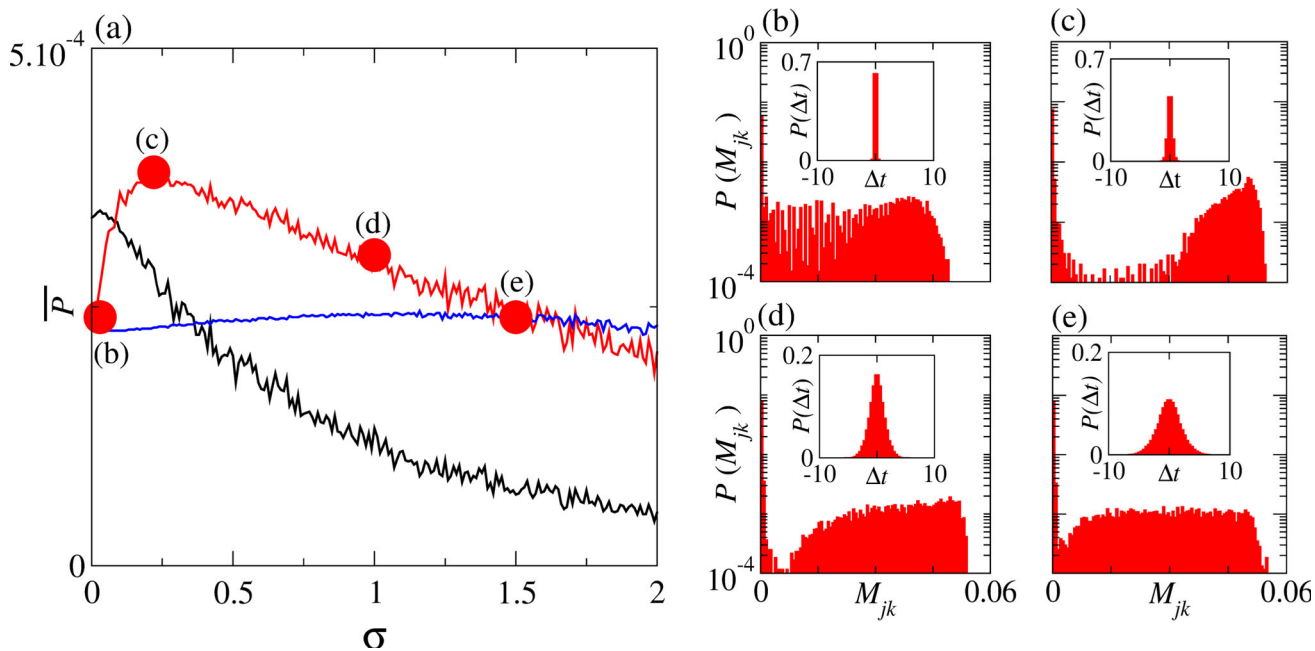


Fig. 5 Measurements of the mean potentiation per spike and the synaptic weights distribution as a function of different variability levels in the phase-synchronous pattern. **a** Mean synaptic weight as a function of the dispersion in the initial condition associated to the parameter σ for the applied constant currents $I_0 = 300$ pA (black line), $I_0 = 500$ pA (red line), and $I_0 = 700$ pA (blue line). The distributions of the synaptic weights for $I_0 = 500$ pA and different values of the dispersion in the initial conditions (σ), indicated in panel **a** by red circles are displayed in the panels **b–e** for $\sigma = 0.03$ pA, $\sigma = 0.22$ pA, $\sigma = 1.0$ pA, and $\sigma = 1.5$ pA, respectively

Fig. 6 Diagnostics of synaptic weight matrices in the parameter space of $\sigma \times I_0$ using the **a** principal component analysis (PCA) and **b** cluster classification (K-means)

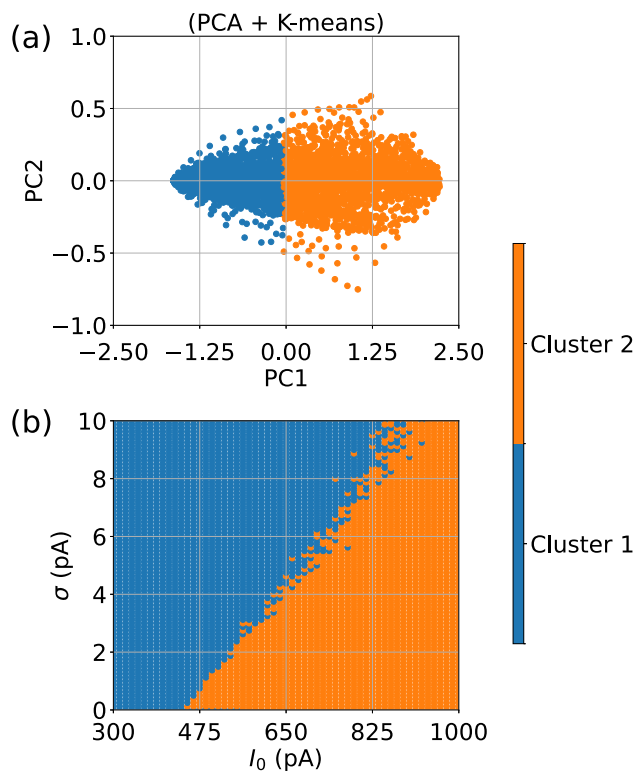
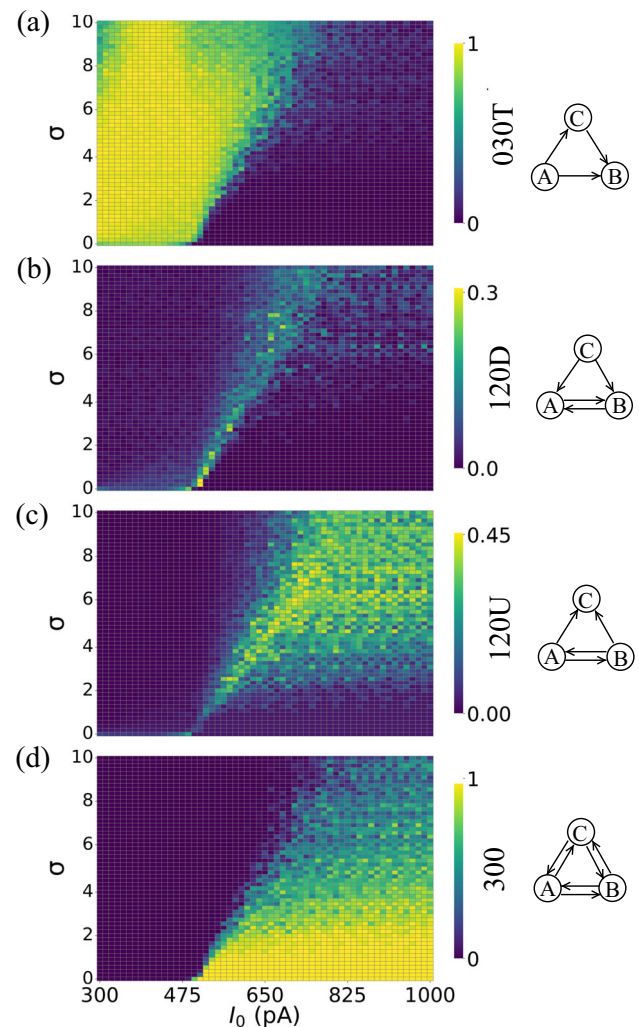


Fig. 7 Percentage of triad structures in the network: **a** 030T, **b** 120D, **c** 120U, and **d** 300



from the simulation in the $\sigma \times I_0$ parameter space. Each matrix of synaptic weights is converted to a one-dimensional vector to represent each network configuration in a high-dimensional feature space. To reduce the data set dimensionality, the PCA was employed. PCA identifies the principal components that exhibit the maximal variance. In this way, it is possible to obtain a low-dimensional representation that exhibits the most significant patterns in the data. After obtaining the low-dimensional space with 10 components, the K-means cluster algorithm was applied to identify the groups of synaptic matrices that have a similar structure. Figure 6 shows the (a) PCA in the principal component 1 (PC1) and principal component 2 (PC2), and the (b) identification of Cluster 1 and Cluster 2 by the K-means method. As suggested by the analysis, the structure in $\sigma \times I_0$ parameter space presents a substantial difference. Particularly, K-means coincides with the characterization of the predominant unidirectional and bidirectional configuration in the $\sigma \times I_0$ space parameter shown in Fig. 4 (f). Such results suggest that beyond the unidirectional and bidirectional connectivity generated in the synaptic connections, some network metrics can have a signature in the synaptic potentiation of these matrices. To clarify the structure observed in $\sigma \times I_0$ parameter space, we further investigated the networks using additional diagnostics.

In Fig. 7, we analyze four triad structures (a) 030T, (b) 120D, (c) 120U, and (d) 300. This measure was done using the Networkx library [54]. The color bars indicate the percentage of triads that conform to each specific triad configuration. The measures considering the directionality of the connections of 3 nodes [55, 56]. To understand the metrics of structure, we consider three nodes (neurons) in the network, named as A , B , and C . If there is a weight connection higher than the initial value from neuron A to B , we establish the representation $A \rightarrow B$. The 030T Triad identifies the proportion of triangular configuration $A \rightarrow C \rightarrow B$, and $A \rightarrow B$, where the arrow indicates the connection direction. The 120D Triad identifies the configuration $A \leftrightarrow B \leftarrow C$ and $C \rightarrow A$. The 120U Triad stands for the structure triad in the form $A \leftrightarrow B \rightarrow C$, and $A \rightarrow C$. The fully connected triad measure, also called as 300 Triad, identifies the structures with six connections between three nodes, i.e., all possible connections between the nodes. Using these measurements, we map where the triad structures are mainly concentrated in

the space parameter of $\sigma \times I_0$. 030T Triads are concentrated in a unidirectional region. 120D Triads are found between the unidirectional and bidirectional regions. 120U Triads are observed in the bidirectional region for high variability of firings. A 300 Triad that represents the fully connected triad is observed in the bidirectional region for low variability of the firings.

5 Discussion and conclusion

The brain exhibits a vast number of activities from synchronous to asynchronous patterns [14, 49]. We have investigated here the influence of transient synchronous and desynchronous activity in the potentiation of synaptic connections by considering a neuronal network composed of excitatory neurons in the presence of spike timing-dependent plasticity. The main motivation for considering only excitatory neurons is to isolate the role of spike variability and spike timing-dependent plasticity in the potentiation of excitatory connections. In addition, the predominance of excitatory connections in certain cortical and hippocampal regions supports the use of the excitatory network as a simplified but biologically relevant approach. In the future, we plan to extend our work to neuronal network with more biological details, including different synaptic types. With our simulations, we have found that the potentiation of the excitatory synaptic connections in unidirectional and bidirectional configurations depends on the firing frequency and the variability of phase-synchronous patterns.

Previous works suggest that connectivity can reflect the firing patterns between neuronal groups in neuronal models with STDP [50]. Clopath et al. reported that the strongest connections may emerge as unidirectional, while bidirectional ones were found in neurons with high spike frequencies [51]. In this work, we have shown that a low spike frequency predominantly potentiates in an unidirectional topology, while a high frequency in a bidirectional one. Furthermore, the increase in the variability of phase synchronization can reduce the fraction of synaptic connections that potentiates in a bidirectional way. Popovych et al. verified that neuronal oscillatory populations with an adaptive synaptic weight can optimize the synaptic increase due to the influence of noise [46]. We have found that such optimization derives directly from a certain level of variability of neuronal spikes. For low firing rates and low dispersion in the phase synchronization, we find a region with a high rate of potentiation per spike. This high rate of potentiation is predominantly associated with unidirectional connections between two and three neurons structures. Depending on the firing frequency, we can also observe a potentiation per spike at a maximal value for a certainly intermediate dispersion of phase synchronization. This fact highlights that a certain level of spike variability can play a constructive role in enhancing synaptic efficacy. In another way, a large variability in phase-synchronous patterns does not appear to contribute efficiently to the synaptic potentiation in bidirectional topologies.

Furthermore, we have elucidated how synchronous levels are associated with changes in the synaptic conductance. If a low level of variability is considered in the phase-synchronous pattern, the number of connections potentiated is reduced. For high dispersion associated with desynchronous patterns, the major part of connections is maintained with a small weight or depressed to zero value. In this case, some connections are strongly potentiated due to statistical coincidences on the spike times [52]. Particularly, we are able to identify the formation of different triads, expanding our understanding of the structure created by STDP.

Considering a more complex neuronal model, such a Hodgkin–Huxley model, the results should remain similar given the same level of phase synchronization. In general, the main results do not depend on the model, but depend on the firing pattern and dispersion of the phase-synchronous activities. In our study, we consider the neuronal activity as a regular spike observed in pyramidal neurons described by the AEIF model. For other models that showed regular spikes with similar activity, we expect the same general pattern of potential dependence on synaptic connections. The results depend strongly on the firing patterns and the synaptic learning rule, not on the model itself. In other words, for other models presenting a comparable spike frequency, adaptation and firing pattern in the presence of STDP, the synaptic potentiation on the excitatory connections should remain consistent. In addition, similar results can be observed for networks of different sizes. To reproduce these findings, adjustments in the initial synaptic weight according to the relation $w_{ij} = 0.1/N$, as well as a reduction of the number of connections per neuron, among other parameters, may be necessary. Adjusting that, we maintain the predominant influence of the firing pattern on the network structure changes, allowing the replication of the results for different network sizes. In this context, our results highlight the importance of the firing frequency and variability in the phase-synchronous patterns in the potentiation of the synaptic connections and on the organization of neuronal networks in the presence of STDP. As a final application, these results suggest that the use of external perturbations to control the neuronal dynamics, which can modify the neuronal structure in a specific way.

Acknowledgements The authors acknowledge the financial support from São Paulo Research Foundation (FAPESP, Brazil) (Grants N. 2020/04624-2, 2023/12863-5, 2024/05700-5, and 2025/02318-5) and support from the Brazilian Federal Agencies (CNPq) under Grant No. 302665/2017-0, 304616/2021-4, 446188/2024-7, 446688/2024-0, 315299/2025-8, 315055/2025-1. D.L.M.S. received partial financial support from Coordenação de Aperfeiçoamento de Pessoal de Nível Superior—Brasil (CAPES) grant number 88887.849164/2023-00. E.C.G. received partial financial support from Coordenação de Aperfeiçoamento de Pessoal de Nível Superior - Brasil (CAPES)—Finance Codes 88881.846051/2023-01. P.R.P. received partial financial support from Coordenação de Aperfeiçoamento de Pessoal de Nível Superior—Brasil (CAPES)—Finance Codes 88887.102678/2025-00.

Funding The Article Processing Charge (APC) for the publication of this research was funded by the Coordenação de Aperfeiçoamento de Pessoal de Nível Superior - Brasil (CAPES) (ROR identifier: 00x0ma614).

Data Availability The data and code supporting the findings of this study are openly available in the public repository at: https://github.com/Protachevicz/Synaptic_potential_dependence.

Open Access This article is licensed under a Creative Commons Attribution 4.0 International License, which permits use, sharing, adaptation, distribution and reproduction in any medium or format, as long as you give appropriate credit to the original author(s) and the source, provide a link to the Creative Commons licence, and indicate if changes were made. The images or other third party material in this article are included in the article's Creative Commons licence, unless indicated otherwise in a credit line to the material. If material is not included in the article's Creative Commons licence and your intended use is not permitted by statutory regulation or exceeds the permitted use, you will need to obtain permission directly from the copyright holder. To view a copy of this licence, visit <http://creativecommons.org/licenses/by/4.0/>.

References

1. A. Morrison, M. Diesmann, W. Gerstner, Phenomenological models of synaptic plasticity based on spike timing. *Biol. Cybern.* **98**, 459–478 (2008)
2. S.B. Brzosko, O.P. Mierau, Neuromodulation of spike-timing-dependent plasticity: Past, present, and future. *Neuron* **103**, 563–581 (2019)
3. A. Citri, R.C. Malenka, Synaptic plasticity: multiple forms, functions, and mechanisms. *Neuropsychopharmacology* **33**, 18–41 (2008)
4. D.O. Hebb, *The organization of behavior: A neuropsychological theory* McGill University (1949)
5. W. Gerstner, W. Kistler, *Spiking neuron models: Single neurons, populations, plasticity* (Cambridge University Press, New York, 2002)
6. G. Bi, A. Poo, Synaptic modification by correlated activity: Hebb's postulate revisited. *Annu. Rev. Neurosci.* **24**, 139–166 (2001)
7. G. Testa-Silva, M.B. Verhoog, N.A. Goriounova, A. Loebel, J. Hjorth, J.C. Baayen, C.P.J. de Kock, H.D. Mansvelder, Human synapses show a wide temporal window for spike-timing-dependent plasticity. *Frontiers in Synaptic Neuroscience* **2**, (2010)
8. E.L. Louth, R.L. Jorgensen, A.R. Korshoej, J.C.H. Sorensen, M. Capogna, Dopaminergic neuromodulation of spike timing dependent plasticity in mature adult rodent and human cortical neurons. *Front. Cell. Neurosci.* **15**, 668980 (2021)
9. G.Q. Bi, M.M. Poo, Synaptic modifications in cultured hippocampal neurons: Dependence on spike timing, synaptic strength, and postsynaptic cell type. *J. Neurosci.* **18**, 10464–10472 (1998)
10. W. Seiger, Synchronization of cortical activity and its putative role in information processing and learning. *Annu. Rev. Physiol.* **55**(1), 349–374 (1993)
11. W. Klimesch, R. Freunberger, P. Sauseng, W. Gruber, A short review of slow phase synchronization and memory: evidence for control processes in different memory systems? *Brain Res.* **1235**, 31–44 (2008)
12. T. Womelsdorf, P. Fries, The role of neuronal synchronization in selective attention. *Current Opinion in Neurobiology* **17**, 154–160
13. S. Grover, J.A. Nguyen, R.M. Reinhart, Synchronizing brain rhythms to improve cognition. *Annual Review of Medicine* **72**, 29–43
14. J. Fell, N. Axmacher, The role of phase synchronization in memory processes. *Nature Reviews Neuroscience* **12**, 105–118
15. M. Kawasaki, K. Kitajo, Y. Yamaguchi, Fronto-parietal and frontotemporal theta phase synchronization for visual and auditory-verbal working memory. *Frontiers in Psychology*
16. L. Melloni, C. Molina, M. Pena, D. Torres, W. Singer, E. Rodriguez, Synchronization of neural activity across cortical areas correlates with conscious perception. *Journal of neuroscience* **27**, 2858–2865
17. F. Varela, J.-P. Lachaux, E. Rodriguez, J. Martinerie, The brainweb: phase synchronization and large-scale integration. *Nat. Rev. Neurosci.* **2**, 229–239 (2001)
18. P. Tass, M.G. Rosenblum, J. Weule, J. Kurths, A. Pikovsky, J. Volkman, A. Schnitzler, H.-J. Freund, Detection of n:m Phase Locking from Noisy Data: Application to Magnetoencephalography. *Phys. Rev. Lett.* **81**(15), 3291 (1998)

19. P.J. Uhlhaas, W. Singer, Neural synchrony in brain disorders: relevance for cognitive dysfunctions and pathophysiology. *Neuron* **52**, 155–168 (2006)
20. A.O. Komendantov, S. Venkadesh, C.L. Rees, D.W. Wheeler, D.J. Hamilton, G.A. Ascoli, Quantitative firing pattern phenotyping of hippocampal neuron types. *Sci. Rep.* **9**, 17915 (2019)
21. E.M. Izhikevich, J.A. Gally, G.M. Edelman, Spike-timing dynamics of neuronal groups. *Cereb. Cortex* **14**, 933–944 (2004)
22. W. Wang, G. Pedretti, V. Milo, R. Carboni, A. Calderoni, N. Ramaswamy, A.S. Spinelli, D. Ielmini, Learning of spatiotemporal patterns in a spiking neural network with resistive switching synapses. *Sci. Adv.* **4**, 1–8 (2018)
23. C. Yang, M.S. Santos, P.R. Protachevicz, P.D.C. dos Reis, K.C. Iarosz, I.L. Caldas, A.M. Batista, Chimera states induced by spike timing-dependent plasticity in a regular neuronal network. *AIP Adv.* **12**, 105119 (2022)
24. E.L. Lameu, F.S. Borges, K.C. Iarosz, P.R. Protachevicz, C.G. Antonopoulos, E.E.N. Macau, A.M. Batista, Short-term and spike-timing-dependent plasticity facilitate the formation of modular neural networks. *Commun. Nonlinear Sci. Numer. Simul.* **96**, 105689 (2021)
25. E.L. Lameu, E.E.N. Macau, F.S. Borges, K.C. Iarosz, I.L. Caldas, R.R. Borges, P.R. Protachevicz, R.L. Viana, A.M. Batista, Alterations in brain connectivity due to plasticity and synaptic delay. *European Physical Journal* **227**, 673–682 (2018)
26. R.A.W. Galuske, M.H.J. Munk, W. Singer, Relation between gamma oscillation and neuronal plasticity in the visual cortex. *Proc. Natl. Acad. Sci.* **116**(46), 23317–23325 (2019)
27. M. Copelli, Physics of psychophysics: Stevens and Weber-Fechner laws are transfer functions of excitable media. *Phys. Rev. E* **65**, 060901 (2002)
28. L.L. Gollo, C. Mirasso, V.M. Eguíluz, Signal integration enhances the dynamic range in neuronal systems. *Phys. Rev. E* **85**(4), 040902 (2012)
29. N.F. Rulkov, Regularization of Synchronized Chaotic Bursts. *Phys. Rev. Lett.* **86**(1), 183–186 (2001)
30. N.F. Rulkov, Modeling of spiking-bursting neural behavior using two-dimensional map. *Phys. Rev. E* **65**(4), 041922 (2002)
31. C. Morris, H. Lecar, Voltage oscillations in the barnacle giant muscle fiber. *Biophys. J.* **35**(1), 193–213 (1981)
32. A. Galves, E. Löcherbach, Infinite systems of interacting chains with memory of variable length - A stochastic model for biological neural nets. *J. Stat. Phys.* **151**(5), 896–921 (2013)
33. E.M. Izhikevich, Neural excitability, spiking and bursting. *International Journal of Bifurcation and Chaos* **10**(6), 1172–1266 (2000)
34. A.L. Hodgkin, A.F. Huxley, A quantitative description of membrane current and its application to conduction and excitation in nerve. *J. Physiol.* **117**(4), 500–544 (1952)
35. J.L. Hindmarsh, R.M. Rose, A model of neuronal bursting using three coupled first order differential equations. *Proceedings of the Royal Society B, Biological Sciences* **221**(1222), 87–102 (1984)
36. B. Xu, S. Binczak, S. Jacquir, O. Pont, H. Yahia, Parameters analysis of FitzHugh-Nagumo model for a reliable simulation. 36th Annual International Conference of the IEEE Engineering in Medicine and Biology Society, Chicago, United States. IEEE (2014)
37. L.F. Abbott, Lapique's introduction of the integrate-and-fire model neuron (1907). *Brain Res. Bull.* **50**(5–6), 303–304 (1999)
38. R. Brette, W. Gerstner, Adaptive exponential integrate-and-fire model as an effective description of neuronal activity. *J. Neurophysiol.* **94**, 3637–3642 (2005)
39. P.R. Protachevicz, F.S. Borges, E.L. Lameu, P. Ji, K.C. Iarosz, A.H. Kihara, I.L. Caldas, J.D.S. Jr, M.S. Baptista, E.E.N. Macau, C.G. Antonopoulos, A.M. Batista, J. Kurths, Bistable firing patterns in a neural network model. *Front. Comput. Neurosci.* **13**, 19 (2019)
40. P.R. Protachevicz, F.S. Borges, K.C. Iarosz, M.S. Baptista, E.L. Lameu, M. Hansen, I.L. Caldas, J.D.S. Jr, A.M. Batista, J. Kurths, Influence of delayed conductance on neuronal synchronization. *Front. Physiol.* **11**, 1–9 (2020)
41. Q. Zhang, Y. Zeng, T. Zhang, T. Yang, Comparison between human and rodent neurons for persistent activity performance: A biologically plausible computational investigation. *Frontiers in Systems Neuroscience* **15** (2021)
42. P.R. Protachevicz, K.C. Iarosz, I.L. Caldas, C.G. Antonopoulos, A.M. Batista, J. Kurths, Influence of autapses on synchronization in neural networks with chemical synapses. *Front. Syst. Neurosci.* **14**, 91 (2020)
43. R. Naud, N. Marcille, C. Clopath, W. Gerstner, Firing patterns in the adaptive exponential integrate-and-fire model. *Biol. Cybern.* **99**, 335–347 (2008)
44. A. Destexhe, Z.F. Mainen, T. Sejnowski, *Kinetic models of synaptic transmission* (MIT Press, Cambridge, 1998)
45. N. Brunel, X.-J. Wang, What determines the frequency of fast network oscillations with irregular neural discharges? I. Synaptic dynamics and excitation-inhibition balance. *J. Neurophysiol.* **90**(1), 1–16 (2002)
46. O.V. Popovych, S. Yanchuk, P.A. Tass, Self-organized noise resistance of oscillatory neural networks with spike timing-dependent plasticity. *Sci. Rep.* **3**, 2926 (2013)
47. M.G. Rosenblum, A.S. Pikovsky, J. Kurths, Phase Synchronization of Chaotic Oscillator. *Physical Review Letter* **76**(11), 1804–1807 (1996)
48. Y. Kuramoto, Self-entrainment of a population of coupled non-linear oscillators. *International Symposium on Mathematical Problems in Theoretical Physics.* 420–422 (1975)
49. J.F. Burke, K.A. Zaghoul, J. Jacobs, R.B. Williams, M.R. Sperling, A.D. Sharan, M.J. Kahana, Synchronous and asynchronous theta and gamma activity during episodic memory formation. *J. Neurosci.* **33**, 292–304 (2013)

50. P.R. Protachevicz, F.B. Borges, A.M. Batista, M.S. Baptista, I.L. Caldas, E.E.N. Macau, E.L. Lameu, Plastic neural network with transmission delays promotes equivalence between function and structure. *Chaos, Solitons Fractals* **171**, 113480 (2023)
51. C. Clopath, L. Busing, E. Vasilaki, W. Gerstner, Connectivity reflects coding: a model of voltage-based stdp with homeostasis. *Nat. Neurosci.* **13**, 344–352 (2010)
52. J.A.P. Silveira, P.R. Protachevicz, R.L. Viana, A.M. Batista, Effects of burst-timing-dependent plasticity on synchronous behaviour in neuronal network. *Neurocomputing* **436**, 126–135 (2021)
53. F. Pedregosa, G. Varoquaux, A. Gramfort, V. Michel, B. Thirion, O. Grisel, M. Blondel, P. Prettenhofer, R. Weis, V. Dubourg, J. Vanderplas, A. Passos, D. Cournapeau, M. Brucher, M. Perrot, É. Duchesnay, Scikit-Learn: Machine Learning in Python. *J. Mach. Learn. Res.* **12**(85), 2825–2830 (2011)
54. A.A. Hagberg, D.A. Schult, P.J. Swart, Exploring network structure, dynamics, and function using NetworkX. *Proceedings of the 7th Python in Science Conference (SciPy2008)*, Gäel Varoquaux, Travis Vaught, and Jarrod Millman (Eds), (Pasadena, CA USA), 11-15 (2008)
55. R. Milo, S. Shen-Orr, S. Itzkovitz, N. Kashthan, D. Chklovskii, U. Alon, Network motifs: simple building blocks of complex networks. *Science*, 298, (2002)
56. R. Rezapour, L. Dinh, L. Jiang, J. Diesner, Structural balance in real-world social networks: incorporating direction and transitivity in measuring partial balance. *Soc. Netw. Anal. Min.* **13**, 168 (2024)